Field-Programmable Gate Array-Based Multichannel Measurement System for Interrogating Fiber Bragg Grating Sensors

Tatsuya Yamaguchi, *Member, IEEE*, Keisuke Ishihara, *Student Member, IEEE*, and Yukitaka Shinoda, *Member, IEEE*

***Abstract*— We develop a field-programmable gate array (FPGA)-based multichannel measurement system for sensing multiplexed fiber Bragg gratings (FBGs), using a high-speed wavelength-swept laser. The wavelength-swept laser, operated with Fourier-domain mode locking (FDML), exhibits a sweep frequency of 50.7 kHz and sweep band of ∼60 nm. A breakthrough in multichannel and real-time measurement is achieved by implementing an FPGA with unique parallel-processing circuits. This FPGA enables the implementation of a high-speed centroid-peak–detection circuit for FBG detection, which can be operated with a sampling frequency of 250 MHz. In multichannel measurement systems, the light propagating through each sensor path produces a delay, which reduces the measurement accuracy. This can be solved by implementing a delay-correction technique, which utilizes the time difference between two spectra obtained by a bidirectional scan of the FDML laser. The system is demonstrated to exhibit multichannel sensing and high measurement time resolution of 9.9 μs, without being affected by the delay.**

***Index Terms*— Field-programmable gate arrays, optical fiber sensors, sensor systems, system integration.**

I. Introduction

FIBER Bragg grating (FBG) sensors have recently been attracting great interest owing to their excellent performances such as high sensitivity, ease of handling, and fast response [1]–[4]. The operating principle of an FBG sensor is that the Bragg wavelength changes according to the changes in the parameters such as strain, temperature, and vibration. In addition, FBGs can be connected serially and multiplexed easily along a single optical fiber. For this reason, there has been considerable interest in the use of FBGs in various applications where high-speed and multipoint measurements are required, such as acoustic emission, sound navigation and ranging, etc. [5]–[9].

Manuscript received February 27, 2019; revised March 24, 2019; accepted March 24, 2019. Date of publication April 3, 2019; date of current version July 3, 2019. The associate editor coordinating the review of this paper and approving it for publication was Dr. Carlos Marques. *(Corresponding author: Tatsuya Yamaguchi.)*

T. Yamaguchi and Y. Shinoda are with the Department of Electrical Engineering, College of Science and Technology, Nihon University, Tokyo 1010062, Japan (e-mail: yamaguchi.tatsuya@nihon-u.ac.jp; shinoda.yukitaka@nihon-u.ac.jp).

K. Ishihara is with the Department of Electrical Engineering, Graduate School of Science and Technology, Nihon University, Tokyo 1010062, Japan (e-mail: cski17005@g.nihon-u.ac.jp).

Digital Object Identifier 10.1109/JSEN.2019.2909105

FBG interrogations using wavelength-swept lasers have been proven to be effective in improving the measurement speed and detection sensitivity [10]–[14]. Wavelength-swept lasers encode the wavelength information of FBGs as time information, and the acquisition timing is determined by the sweep frequency of the wavelength-swept laser. Broadband wavelength-swept lasers can further simplify the multiplexing of FBGs. The Fourier-domain mode locking (FDML) technique has recently overcome the limitations of sweep frequency, and allows high-speed operation, beyond tens of kHz [15]. Taking advantage of the FDML laser, research on high-speed FBG interrogation has demonstrated measurement rates of several tens of kHz [16]–[20]. For further improving the multiplexing capabilities, an approach based on low-reflectance FBGs has been proposed [21]. Several recent studies have focused on improving the performance by introducing optical approaches. The application of optical approaches has resulted in an increase in the processing load of electrical signal-processing systems. The development of high-speed signal-processing systems has been a breakthrough to achieve real-time measurement of FBGs, allowing FBGs to be applied widely in various fields. However, very few studies have reported in detail, high-speed signal-processing systems using high-speed wavelength-swept lasers. Nowadays, field-programmable gate arrays (FPGAs) have been attracting attention as a key evolving technology for improving the performance of signal-processing systems. Introduction of high-speed digital signal processing using FPGAs has been reported to improve dramatically the performance of the systems in various fields such as control and communication [22], [23].

In the measurement with multiplexed FBGs by using a high-speed wavelength-swept laser, it is necessary to consider the influence of the light-propagation time. The measurement system is connected to the FBG sensor by an optical fiber, and the propagation time (delay) is the time taken for the light to pass through the optical fiber. The delay degrades the measurement accuracy of the system, which measures the wavelength information of the FBG as time information. For this reason, delay corrections using a frequency comb or a Fabry–Perot etalon were demonstrated [24], [25].

In this paper, we develop an FPGA-based multichannel measurement system for multiplexed FBGs, which uses an

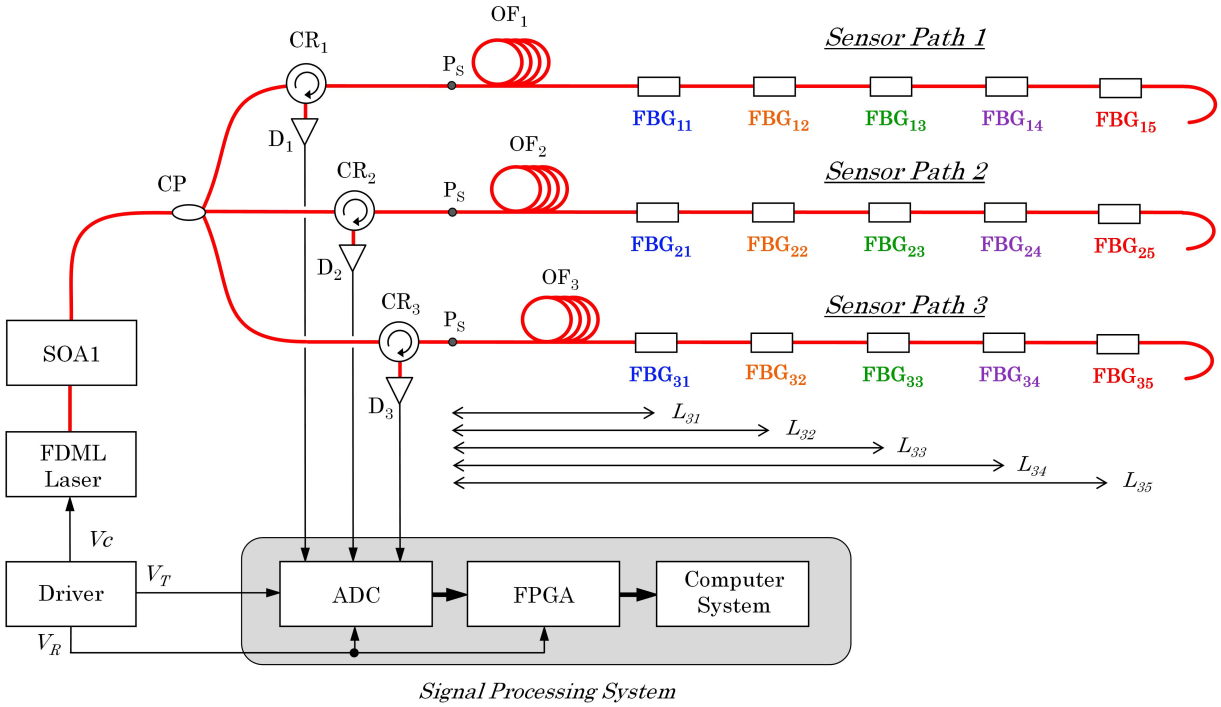

Fig. 1. Multichannel fiber Bragg grating (FBG) interrogation system utilizing field-programmable gate array (FPGA). SOA: Semiconductor optical amplifier; CP: coupler; CR: circulator; Ps: reference position; OF: optical offset fiber; D: detector; ADC: analog-to-digital converter; FPGA: field programmable gate array.

FDML laser [19], [20]. The FDML laser operates with a sweep frequency of 50.7 kHz, sweep band of ∼60 nm, and output power of ∼1.4 mW. The signal-processing system implements an FPGA, for performing real-time high-speed digital calculations. The unique centroid-peak–detection circuit designed in the FPGA detects the multiplexed FBGs, with precise timing control, at a sampling frequency of 250 MHz. In addition, the signal-processing system introduces a delay-correction method to eliminate the influence of propagation time in the optical fiber connected to the FBG. The correction utilizes the time difference between the two spectra, obtained from the bidirectional scan of the FDML laser, and has the following advantages: no special optical considerations are necessary, low calculation cost for real-time processing, and is applicable to multichannel measurements. The developed measurement system demonstrates that simultaneous multichannel measurement with a time resolution of 9.9 μs is possible, without being affected by the delay.

II. System

A. Setup for Multichannel FBG Measurement System

Fig. 1 shows a multichannel FBG measurement system with an FPGA. The optical system consists of an FDML laser, semiconductor optical amplifier (SOA1, SOA1013, Thorlabs), coupler (CP), circulators (CRs), FBG sensors installed in a multiplexed sensor path, and detectors (Ds). The FDML laser is constructed using a semiconductor optical amplifier (SOA2, SOA1117, Thorlabs), a fiber Fabry–Perot tunable filter (FFP-TF, Micron Optics), and a two-kilometer-long optical fiber [19]. Each component of the FDML laser is temperature-controlled, at a temperature of 25 °C. The FFP-TF has a free spectral range of 190 nm and finesse of 2195. The FFP-TF is driven by a sinusoidal signal from the driver and is operated with a sweep frequency f_m of 50.7 kHz. The light emitted from the FDML laser is amplified by the SOA1, which functions as a booster amplifier, and is incident on the sensor paths. Five FBGs are multiplexed in each sensor path ($K = 1$ to 3). FBG_{KJ} ($K = 1$ to 3, $J = 1$ to 5) have Bragg wavelengths of 1530, 1540, 1550, 1560, and 1565 nm, a half width of ∼0.2 nm, and a reflectance of ∼80%. Each FBG is installed at an optical fiber length of L_{KJ} from the reference position $\mathrm{P_S}$ of the system (see Table I). In this case, the delay τ_{KJ} is generated according to the L_{KJ} of each FBG as follows:

$$\tau_{KJ} = \frac{2nL_{KJ}}{c} \quad (K = 1 \text{ to } 3, J = 1 \text{ to } 5), \tag{1}$$

where n is the refractive index of the optical fiber and c is the speed of light. In order to clarify the influence of the delay, an optical offset fiber OF_K ($K = 1$ to 3) can be inserted into each sensor path. Therefore, the L_{KJ} increases by the length L_{OK} ($K = 1$ to 3) of OF_K. The reference position $\mathrm{P_S}$ is the position where the FDML laser's wavelength-sweep characteristics were measured (described in Section III. A). The reflected light from each FBG in each sensor path is received by each D_K ($K = 1$ to 3) via each CR_K ($K = 1$ to 3). The detectors have a frequency range of DC to 250 MHz.

The signal-processing system realizes real-time processing by interlocking the analog-to-digital converter (ADC) equipped with the FPGA (5170R, National Instruments) and

TABLE I
OPTICAL FIBER LENGTH FROM P_S TO EACH FBG WITHOUT OPTICAL OFFSET FIBER

Sensor Path	Grating	Optical Fiber Length L_{KJ} (m)
1	FBG_{11}	4.86
	FBG_{12}	10.28
	FBG_{13}	15.84
	FBG_{14}	21.04
	FBG_{15}	26.55
2	FBG_{21}	5.22
	FBG_{22}	8.54
	FBG_{23}	11.89
	FBG_{24}	15.23
	FBG_{25}	18.55
3	FBG_{31}	5.30
	FBG_{32}	8.62
	FBG_{33}	11.93
	FBG_{34}	15.25
	FBG_{35}	18.57

the computer system. The ADC takes four-channel 14-bit analog inputs, and operates at sampling frequencies up to 250 MHz. In addition, the ADC conforms to the communication standard of JESD204B and provides high-speed data transfer to the FPGA. The FPGA, which supports high-speed mainstream data, can perform onboard signal processing in real-time. For precise adjustment of the timing control, these two devices are operated with a common reference clock V_R of 10 MHz, through a driver. Activated by a trigger signal V_T from the driver, the ADC acquires the detector signals V_{DK} ($K = 1$ to 3) from each FBG, which reflects at its own Bragg wavelength. The peaks of the FBGs are interrogated by the FPGA, which is implemented using parallel-processing circuits designed to support real-time operation. The measurement system is designed with a delay-correction method for sensing multiplexed FBGs. Operated with an FDML laser with a sweep frequency f_m of 50.7 kHz, the measurement system has a measurement time resolution $T_m\left(=1/2f_m\right)$ of 9.9 μs. Experiments demonstrate that the system can perform real-time measurements of multiplexed FBG sensors, without being affected by the delay.

B. FBG Wavelength Measurement With FDML Laser

Fig. 2 shows the schematic diagram explaining the wavelength measurement of the FBG using the FDML laser. The FDML laser performs a forward scan (scanning in sweep from short wavelength to long wavelength) and backward scan (scanning in sweep from long wavelength to short wavelength), sinusoidally. It is assumed that the Bragg wavelength of the FBG is λ_{FBG} and that the installation position of the FBG is the reference position P_S of the measurement system shown in Fig. 1. In this case, the delay τ is absent because there is no optical fiber connected to the FBG. The reflection spectra of the FBG appear at t_{FS} in the forward scan and t_{BS} in the backward scan, when the wavelength of the laser coincides with the wavelength of the FBG. The reflection wavelength

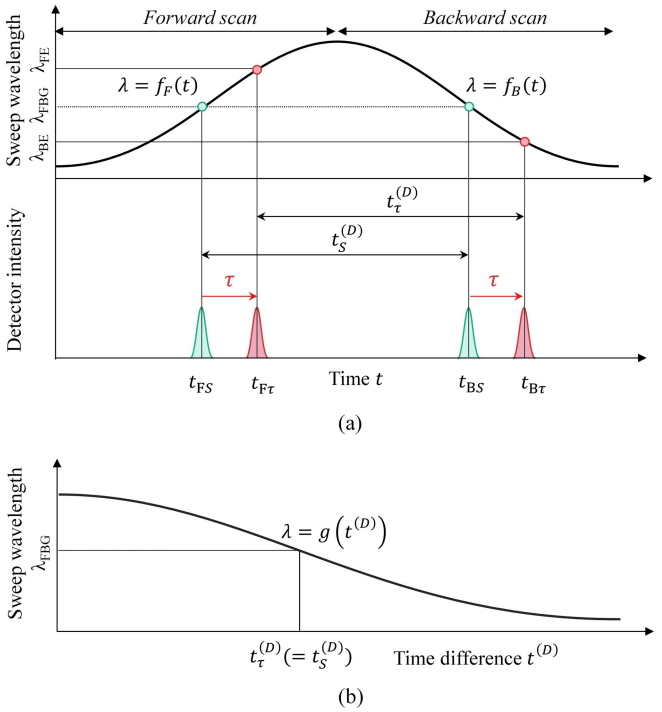

Fig. 2. Concept for measuring fiber Bragg grating (FBG) with wavelength swept laser. (a) Fiber Bragg grating (FBG) signal with wavelength-swept laser. (b) Relationship between time difference and sweep wavelength.

of the FBG can be calculated by substituting the obtained reflection spectrum times t_{FS} and t_{BS} into the wavelength sweep characteristics: $f_F(\cdot)$ in the forward scan and $f_B(\cdot)$ in the backward scan.

$$\lambda_{FBG} = f_F(t_{FS}) \tag{2}$$

$$\lambda_{FBG} = f_B(t_{BS}) \tag{3}$$

When the delay is not included, the reflection wavelengths of the FBG in the forward and backward scans have equal values. On the other hand, if the FBG is assumed to be installed at a position, which is an optical fiber length L away from the reference position P_S, a delay τ will be produced. The reflection spectra of the FBG will shift and will be obtained at times of $t_{F\tau}$ and $t_{B\tau}$. Therefore, as shown in Fig. 2(a), the calculated wavelength will be shifted from the original wavelength as follows:

$$\lambda_{FE} = f_F(t_{F\tau}), \tag{4}$$

$$\lambda_{BE} = f_B(t_{B\tau}), \tag{5}$$

where λ_{FE} and λ_{BE} are the wavelengths affected by the delay in the forward and backward scans, respectively. Therefore, we propose a method to correct the delay by using the time difference of the reflection spectra of the FBG, obtained from the forward and backward scans. As shown in Fig. 2(a), the time difference is constant at $t_\tau^{(D)} = t_S^{(D)}$, regardless of the presence or absence of delay, and it varies depending on the wavelength alone, without being affected by the delay. Fig. 2(b) shows the wavelength-sweeping characteristic

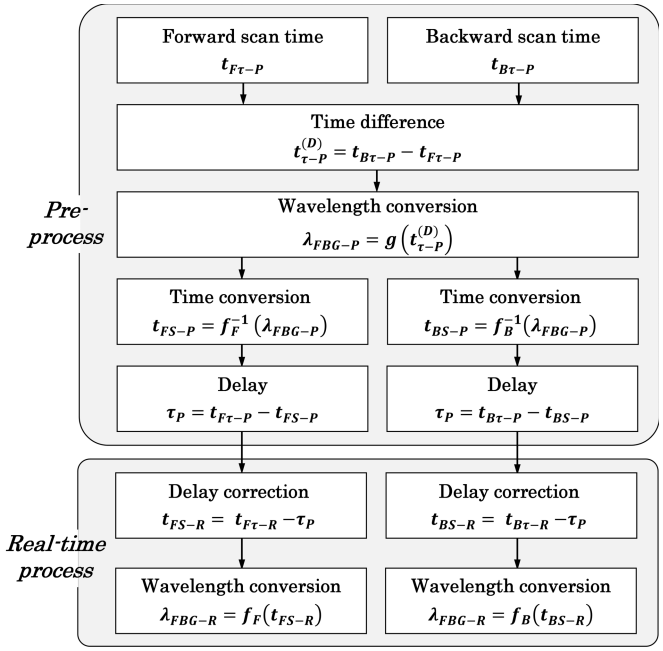

Fig. 3. Calculation flow of fiber Bragg grating (FBG) wavelength with delay correction method.

$g(\cdot)$ based on the relationship between the time difference and sweep wavelength.

C. Delay Correction

Fig. 3 shows a flow of processing for correcting the delay by utilizing the time difference. The processing is divided into preprocessing and real-time processing (indicated by the suffixes P and R). First, in preprocessing, a time difference $t_{\tau-P}^{(D)}$, which is affected by the delay, is calculated from the reflection spectrum times $t_{F\tau-P}$ in the forward scan and $t_{B\tau-P}$ in the backward scan. From the time difference, the wavelength λ_{FBG-P} is calculated using the wavelength-sweep characteristic $g(\cdot)$ of the time difference. The result is the original wavelength of the FBG, which is not affected by the delay. Therefore, the wavelength λ_{FBG-P} makes it possible to estimate the reflection spectrum times t_{FS-P} and t_{BS-P}, by using the inverse functions $f_F^{-1}(\cdot)$ and $f_B^{-1}(\cdot)$ in the wavelength-sweep characteristics. Thus, by this processing, the delay τ_P is calculated. In the real-time processing step, by using this delay τ_P, the influence of delay on the reflection spectrum times $t_{F\tau-R}$ and $t_{B\tau-R}$ measured in the forward and backward scans is measured and the reflection spectrum times are corrected as t_{FS-R} and t_{BS-R}. Finally, the wavelengths λ_{FBG-R} are calculated, without being affected by the delay. In this calculation flow, since preprocessing produces an estimation of the delay, real-time processing can easily perform the corrections by merely subtracting the delay from the obtained spectrum. Therefore, this correction method has the following merits: a special optical system for correction is not required, the calculation cost for real-time processing is low, and it is applicable to multiplexed channels. In this processing method, since the wavelength can be calculated by both the forward and backward scans, the measurement time resolution T_m can be improved to $1/2f_m$.

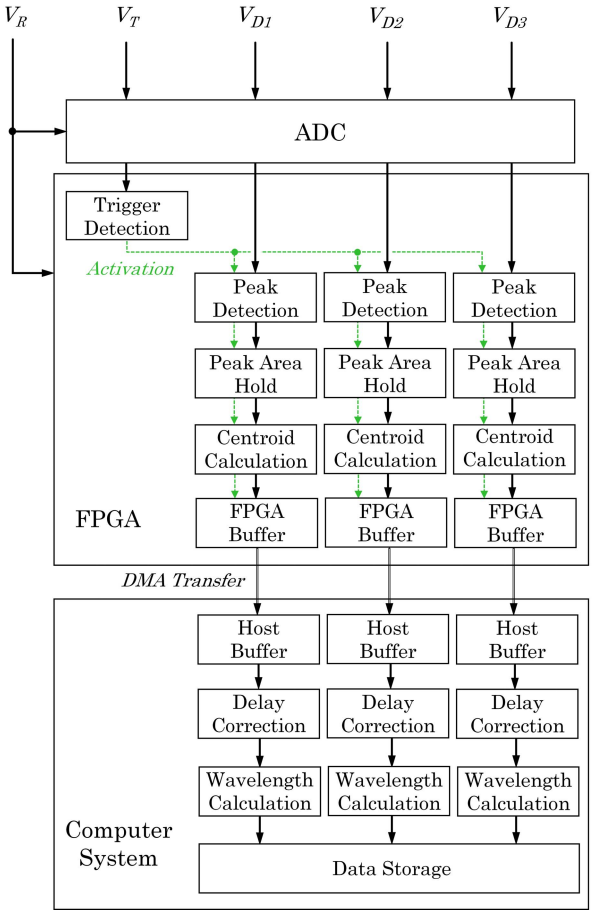

Fig. 4. Data flow for signal-processing system.

D. Design of Signal-Processing System

To achieve real-time FBG signal detection when operating a high-speed wavelength-swept laser, a high-throughput signal-processing system is required. This demand is resolved by installing an FPGA, which can accept data transfers at rates above several Gb/s and reduce the processing load on the CPU during real-time operation. The signal-processing system is designed using the graphical programming language of LabVIEW (National Instruments). Fig. 4 shows the system design for the signal processing. The ADC acquires and transfers the detector signals V_{DK} ($K = 1$ to 3) and the trigger signal V_T to the FPGA, with a sampling frequency of 250 MHz.

The FPGA comprises internal circuits for trigger detection and FBG signal detection processing. The trigger-detection function detects the trigger signal V_T synchronized with the FDML laser, and when it becomes valid, it shifts the FBG signal-detection processing from the idle state to the active state. In the FBG signal-detection processing, a detection method based on centroid calculation is introduced in order to achieve high resolution in peak detection. The FBG signal-detection processing consists of a peak-detection function, data-holding function, and centroid-calculation function. The peak-detection function obtains the data in which the

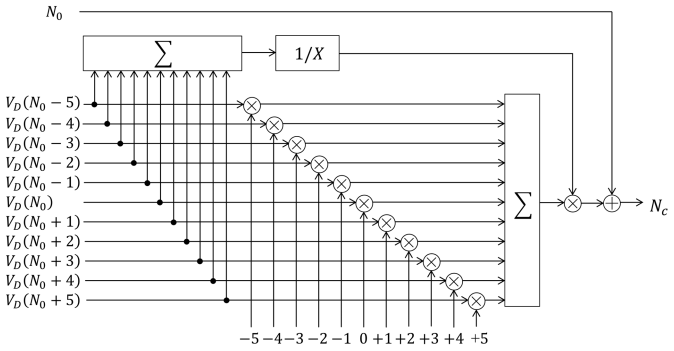

Fig. 5. Design of centroid calculation function in FPGA.

amplitude value of the FBG signal is the peak. The data-holding function holds the acquired peak data and the surrounding data. The centroid-calculation function calculates the centroid position N_{CKJ} of each FBG_{KJ} as expressed by (6), using the held data.

$$N_{CKJ} = \frac{\sum_{i=N_{0KJ}-M_m}^{N_{0KJ}+M_m} V_{DK}(i) \times i}{\sum_{i=N_{0KJ}-M_m}^{N_{0KJ}+M_m} V_{DK}(i)} \quad (K = 1 \text{ to } 3,\ J = 1 \text{ to } 5), \tag{6}$$

where N_0 is the data number of the peak value and M_m is the number that holds the data before and after the peak value.

Fig. 5 shows the circuit design for implementing the centroid-calculation function of the FPGA. The four arithmetic operations are constructed using high-throughput math functions corresponding to fixed-point operations, which are provided by National Instruments. The four arithmetic operations have a built-in handshake facility for establishing synchronous data transfer between math functions. In addition, the bit length associated with the operation can be adjusted automatically, and it operates without overflow. Furthermore, since it uses a fixed point, it operates with less resources. Fig. 5 shows a mounting circuit for the case where $M_m = 5$ in the centroid-calculation function. Eleven data acquired by the data-holding function pass through each data line and are input to the arithmetic functions. The input data are processed by each calculation function, and the centroid position N_C is calculated.

The configuration functions inside the FPGA of Fig. 4 are subroutineized. Therefore, the programming for parallel processing can be implemented easily, and can easily cope with the expansion of the sensor path. The calculated results for the centroid position of each FBG are input sequentially to a first-in-first-out (FIFO) buffer in each detector channel, and are transferred to the computer system by direct memory access (DMA). In the computer system, the transferred data are converted from the data number N_C to the time t_C. Then, delay correction and wavelength conversion are performed on the transferred data, and the measurement result is reflected on the developed display system (Fig. 6). The display system consists of a control panel and monitor for measurement. On the monitor, the FBG of each sensor path can be displayed

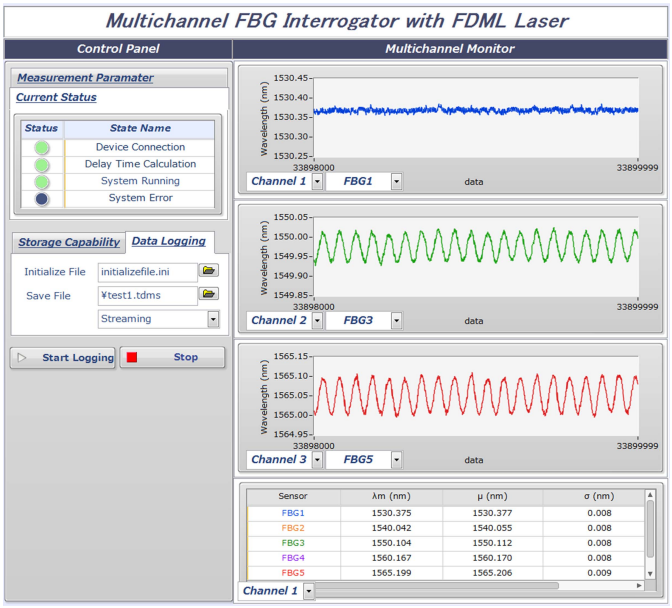

Fig. 6. Screen of the measurement system.

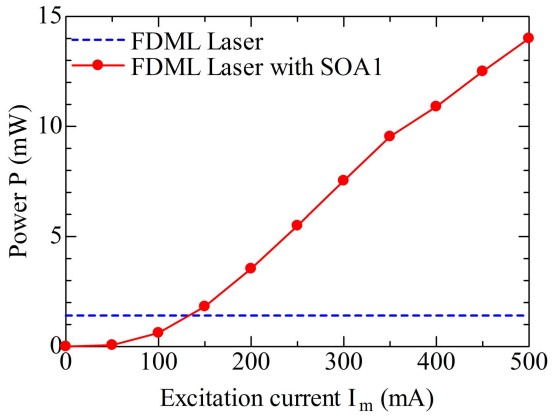

Fig. 7. Output power of FDML laser.

in real-time, and it can be observed for the range from static strain to high-speed vibration.

III. Measurement Results

A. Characteristics of FDML Laser

The optical power of the FDML laser was measured using an optical power meter. Fig. 7 shows the results of the optical output of the FDML laser according to the presence or absence of SOA1 in Fig. 1. When using the FDML laser alone, the light output is ∼1.4 mW. In the case of using SOA1, the optical output of the FDML laser is amplified on increasing the excitation current. When the excitation current is 500 mA, an optical output of ∼14 mW is obtained, and SOA1 functions as a booster amplifier. Fig. 8 shows the output spectrum of the FDML laser, obtained using an optical spectrum analyzer with averaging times of 100. The FDML laser has a center wavelength of 1550 nm and sweep band of 60 nm. The FDML laser operates at a sweep frequency of 50.7 kHz and performs high-speed wavelength sweeping. SOA1, with an

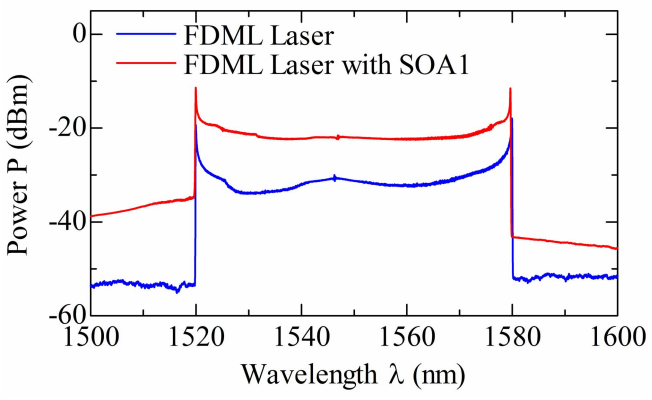

Fig. 8. Spectrum of wavelength sweeping in FDML laser.

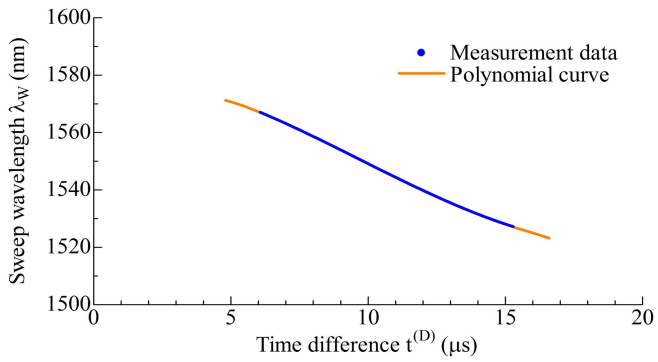

Fig. 9. Characteristic for wavelength sweeping in time difference.

excitation current of 500 mA, amplifies the light output, which increases to ∼7.5 dBm at the center wavelength. In FBG measurement, SOA1 is operated with an excitation current of 500 mA.

The wavelength-sweep characteristics of the FDML laser were measured using an optical system with an optical tunable filter (FFM-C, Axsun Technologies) and a wavelength monitor (FB200, Ando) [19]. The wavelength monitor has a measurement range of 1527 to 1567 nm and a wavelength resolution of 1 pm. The experiment was performed with the optical fiber length corresponding to the reference position P_S in Fig. 1. The output light of the FDML laser is incident on the optical tunable filter, and the transmitted light is measured by the detector and the wavelength monitor. The experiment exhibits the correspondence between the time and the wavelength of the FDML laser. Therefore, by tuning the wavelength with optical tunable filter, spectrum times t_{FS} and t_{BS} were measured as shown in Fig. 2. Using these results, the polynomial curve for the wavelength-sweep characteristics $f_F(\cdot)$ in the forward scan and $f_B(\cdot)$ in the backward scan was calculated. The standard deviation of the differences between the measured values and the polynomial values was less than $\sim 4 \times 10^{-2}$ nm. The time difference $t^{(D)}$ of the two spectrum times for obtaining the wavelength-sweep characteristic $g(\cdot)$ was also measured.

Fig. 9 shows the wavelength-sweep characteristic of the FDML laser, with respect to the time difference. The wavelength changes according to the change in the time difference.

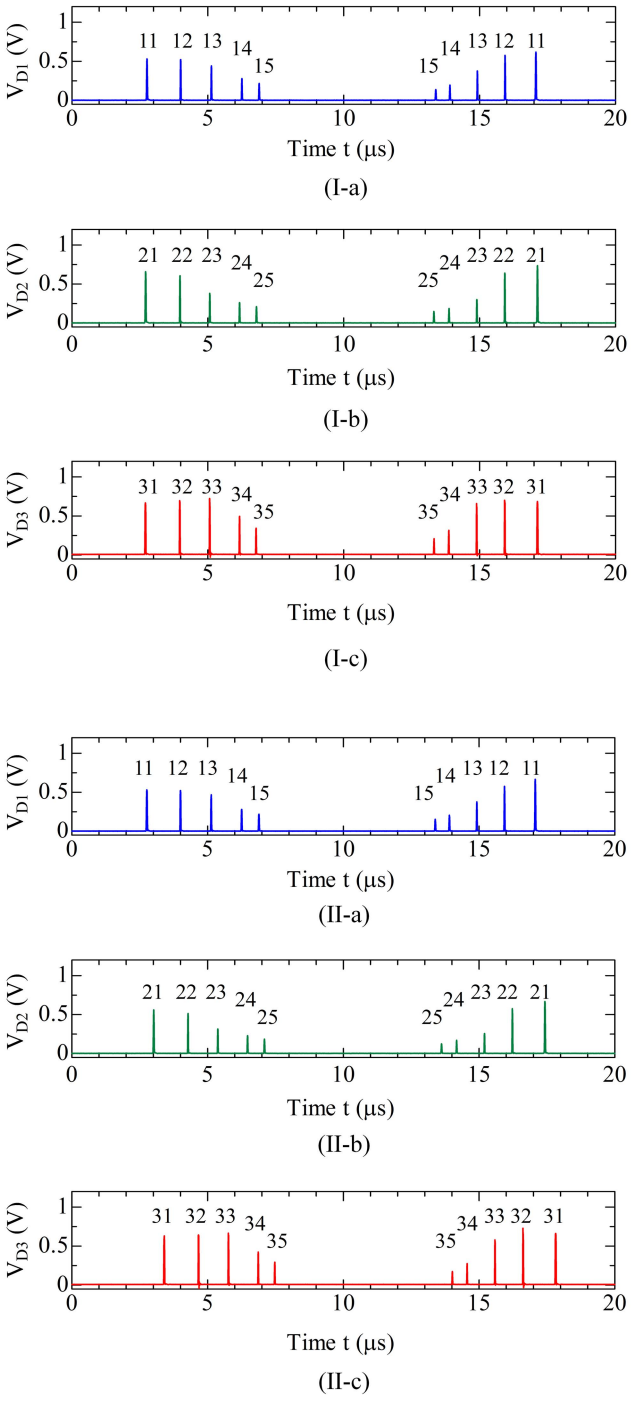

Fig. 10. Fiber Bragg grating (FBG) reflection signal in wavelength sweeping. (I) Reflection signals without optical offset fiber, (I-a) sensor path 1 ($L_{O1} = 0$ m), (I-b) sensor path 2 ($L_{O2} = 0$ m) and (I-c) sensor path 3 ($L_{O3} = 0$ m). (II) Reflection signals with optical offset fiber, (II-a) sensor path 1 ($L_{O1} = 0$ m), (II-b) sensor path 2 ($L_{O2} = 30$ m) and (II-c) sensor path 3 ($L_{O3} = 70$ m).

The polynomial curve was calculated from the results obtained in this experiment, and was used for obtaining the wavelength-sweep characteristic $g(\cdot)$ for the time difference $t^{(D)}$. In addition, the delay correction was performed according to the processing flow of Fig. 3, using the results of the wavelength-sweep characteristics.

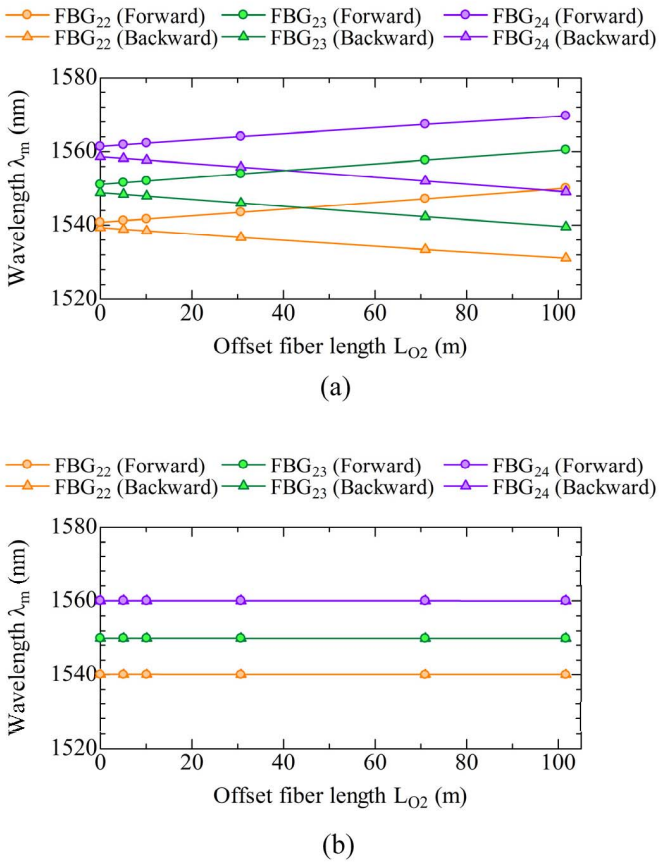

Fig. 11. Influence of measuring wavelength on delay. (a) Case affected by delay. (b) Case of correcting delay.

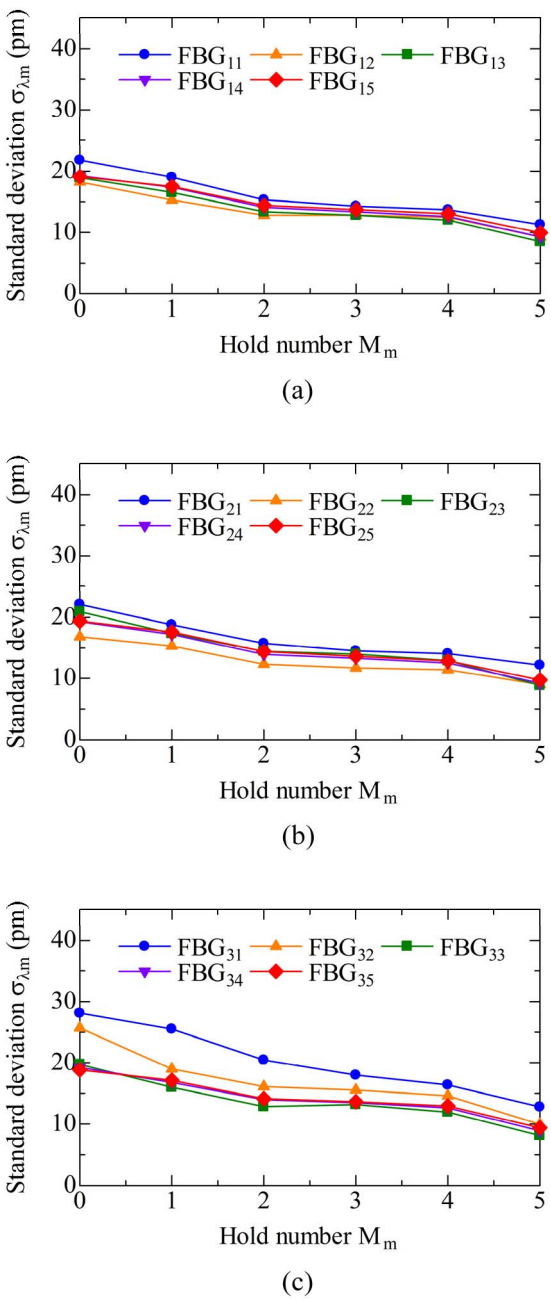

Fig. 12. Wavelength measurement with centroid-calculation function. (a) Sensor path 1. (b) Sensor path 2. (c) Sensor path 3.

B. FBG Detection and Delay Correction

The reflection signals of the FBG measured using this system are shown in Fig. 10. Fig. 10 (I-a) to (I-c) are the detector signals V_{DK} ($K = 1$ to 3) of each sensor path. The length of the optical offset fiber OF_K ($K = 1$ to 3) of each sensor path was set to $L_{OK} = 0$ m ($K = 1$ to 3). The FDML laser sweeps the wavelength for one cycle ($1/f_m$) in the forward and backward scans. The reflected signal of each installed FBG_{KJ} ($K = 1$ to 3, $J = 1$ to 5) can be detected in each sensor path. The detection interval of the FBG is 9.9 μs, in each sweep of the FDML laser. Fig. 10 (II-a) to (II-c) show the results when the OF_K of each sensor path is set to $L_{O1} = 0$ m, $L_{O2} = 30$ m, and $L_{O3} = 70$ m, respectively. In Fig. 10 (II-b) and Fig. 10 (II-c), the reflected signals of the FBG are observed to have been delayed by 0.30 μs and 0.70 μs, compared to that in Fig. 10 (I-b) and Fig. 10 (I-c), respectively. The reflected signals are influenced by the delays due to the optical fiber lengths.

Thus, the effect of delay on the wavelength measurement was evaluated. Fig. 11 shows the results of calculating the wavelengths of FBG_{22}, FBG_{23}, and FBG_{24}. Fig. 11 (a) shows the measurement results of the case affected by the delay. A problem is observed wherein the wavelength of each FBG is measured to have been shifted from the original wavelength to the long-wavelength side in the forward scan and short-wavelength side in the backward scan, owing to the influence of the delay for an increase of L_{O2} of OF_2. The wavelength shifts due to such a delay can cause a discrimination error in the FBG. For example, when the original wavelength of FBG_{22} is 1540 nm and $L_{O2} = 101.68$ m, the measured wavelength may be observed as 1550.09 nm in the forward scan, and there is a possibility that the wavelength may be erroneously recognized as that of FBG_{23}, which has an original wavelength of 1550 nm. Even when $L_{O2} = 0$ m, the optical fiber lengths to the respective FBGs are $L_{22} = 8.54$ m, $L_{23} = 11.89$ m, and $L_{24} = 15.23$ m (Table I); therefore, each wavelength is shifted and measured as $\lambda_{m22} = 1540.77$ nm, $\lambda_{m23} = 1551.09$ nm, and $\lambda_{m24} = 1561.39$ nm during the forward scan, and $\lambda_{m22} = 1539.32$ nm, $\lambda_{m23} = 1548.92$ nm, and $\lambda_{m24} = 1558.62$ nm during the backward scan.

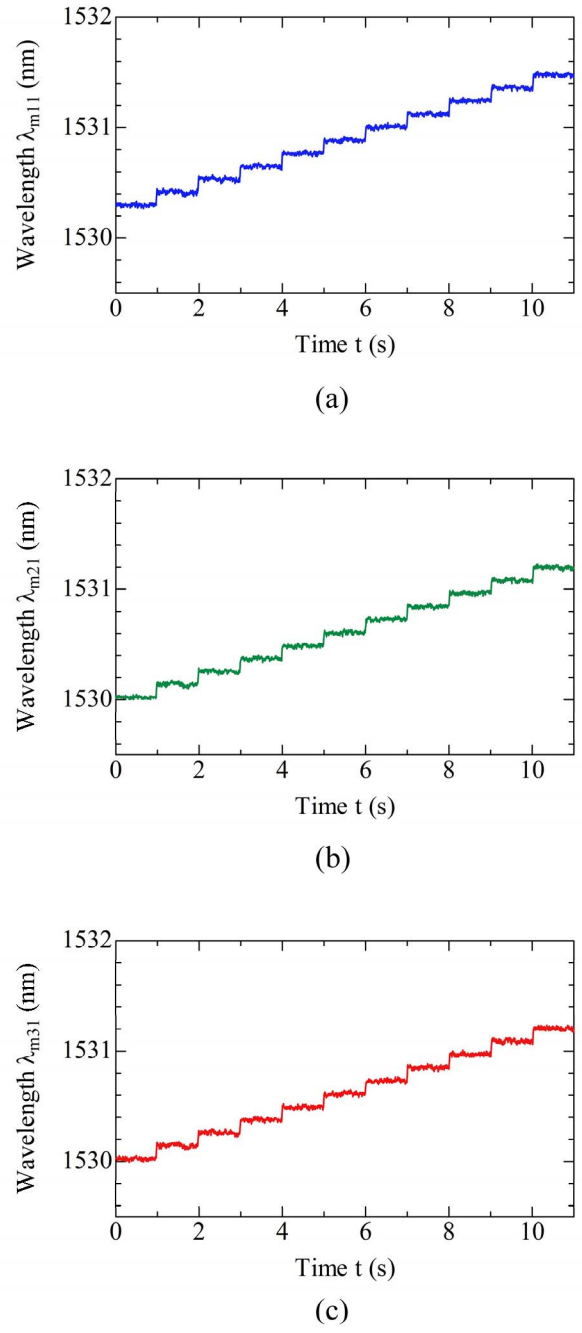

Fig. 13. Multichannel sensing for static strain measurement. (a) Sensor path 1 (FBG_{11}) ($L_{O1} = 0$ m). (b) Sensor path 2 (FBG_{21}) ($L_{O2} = 30$ m). (c) Sensor path 3 (FBG_{31}) ($L_{O3} = 70$ m).

In order to solve this problem, Fig. 11 (b) shows the result of measuring the wavelength by introducing the delay-correction method shown in Fig. 3. The wavelengths of the FBGs, measured in the forward and backward scans are approximately equal and in agreement with $\lambda_{m22} = 1540.05$ nm, $\lambda_{m23} = 1550.00$ nm, and $\lambda_{m24} = 1560.01$ nm, regardless of the delay in L_{O2}. Even when $L_{O2} = 0$ m, the influence of the initial optical fiber length shown in Table I can be cancelled. Introduction of this correction process enables delay-correction and real-time measurement.

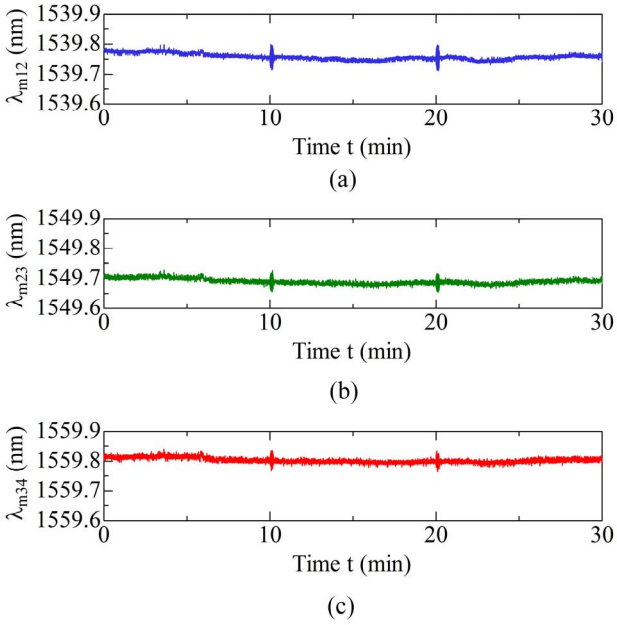

Fig. 14. Long-time wavelength measurement in real-time. (a) Sensor path 1 (FBG_{12}). (b) Sensor path 2 (FBG_{23}). (c) Sensor path 3 (FBG_{34}).

C. Wavelength Measurement With Centroid-Calculation Function

The reflection wavelength measurement of the FBG uses a peak-detection process based on the centroid-calculation function, as shown in Fig. 12. Fig. 12 (a) to (c) show the results of each sensor path, and the standard deviation of the reflected wavelength measured for one second is calculated. M_m represents the number of data held in the centroid-calculation function of (6). The case where $M_m = 0$ is the result of direct peak detection, and the standard deviation value of the FBG is 28 pm at the maximum. When M_m is increased, the value of the standard deviation of the reflection wavelength is improved. When $M_m = 5$, the maximum value is 13 pm. From these results, it can be inferred that the centroid-calculation function using the FPGA operates as a high-speed digital circuit, achieving real-time detection of FBG and high measurement-wavelength resolution. In this system, calculation functions with $M_m = 5$ are implemented in parallel, enabling multichannel measurement of 15 FBGs.

D. Multichannel and Real-Time Measurement

We evaluated the multichannel measurement of the reflected wavelength due to static strain. Fixed stages and movable stages (SGSP-26-100, SIGMAKOKI) were attached to both ends of the optical fibers of FBG_{11}, FBG_{21}, and FBG_{31} in each sensor path, and the interval of the two stages, L_{stage}, was set to 1 m. When the movable stage was moved by $\Delta L_M \mu$m, a strain $\Delta\varepsilon(= \Delta L_M/L_{stage})\mu\varepsilon$ was applied. A strain of 100 $\mu\varepsilon$ was applied repeatedly to each FBG, every second. Note that the OF_K ($K = 1$ to 3) of each sensor path was set to $L_{O1} = 0$ m, $L_{O2} = 30$ m, and $L_{O3} = 70$ m. Fig.13 (a) to (c) are the results of the reflection wavelength measurements of FBG_{11}, FBG_{21}, and FBG_{31} in each sensor path. Using bidirectional sweeping, the system can measure step

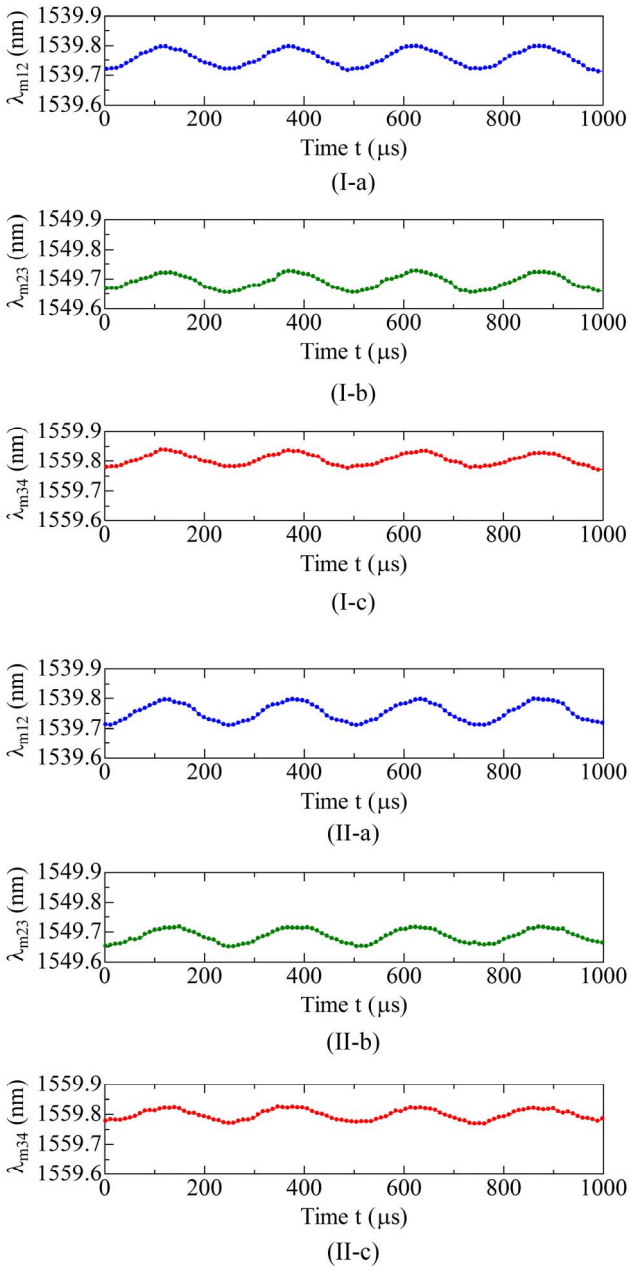

Fig. 15. Enlarged view of Fig. 14. (I) Over 10 min, (I-a) sensor path 1 (FBG_{12}), (I-b) sensor path 2 (FBG_{23}) and (I-c) sensor path 3 (FBG_{34}). (II) Over 20 min, (II-a) sensor path 1 (FBG_{12}), (II-b) sensor path 2 (FBG_{23}) and (II-c) sensor path 3 (FBG_{34}).

changes in the reflected wavelength due to the application of strain in each FBG. Furthermore, even when there is an influence of the delay, the system can measure the reflected wavelength of the original FBG using the correction processing. The amount of change in the reflected wavelength per strain step of each FBG was $\sim 12 \times 10^{-2}$ nm. The sensitivity of the reflection wavelength to the strain was $\sim 1.2 \times 10^{-3}$ nm/$\mu\varepsilon$ ($R^2 = 0.9999$). This experiment proves that the influence of the delay can be corrected and that the reflected wavelengths due to the strain can be measured simultaneously by using the FBGs in a system with multiple channels.

Finally, the high-speed real-time measurement of reflection wavelength using instantaneous vibrations was evaluated. FBG_{12}, FBG_{23}, and FBG_{34} of each sensor path were attached to one metal-laminate–type piezoelectric actuator, and vibrations were applied. The vibration frequency of the actuator was set to 4 kHz, and the actuator was operated every 10 min. The OF_K ($K = 1$ to 3) of each sensor path was set to $L_{OK} = 0$ m ($K = 1$ to 3). Fig. 14 (a) to (c) are the measurement results for FBG_{12}, FBG_{23}, and FBG_{34} of the sensor paths. The reflection wavelength of each FBG fluctuates greatly every 10 min, simultaneously, when vibrations are applied. Fig. 15 (I-a) to (I-c) are the results of enlarging the 10-min time regions of Fig. 14 (a) to (c). The reflection wavelength of each FBG can be measured as a sinusoidal vibration with a vibration frequency of 4 kHz. The measurement time resolution was determined 9.9 μs by using both forward and backward scans of the FDML laser driven at a sweep frequency of 50.7 kHz. In FBG_{12}, the fluctuation amount of the wavelength on the application of vibration was $\sim 8 \times 10^{-2}$ nm. Fig. 15 (II-a) to (II-c) are the results of enlarging the 20 min time regions of Fig. 14 (a) to (c). The change in the reflection wavelength of each FBG can be observed to be the same as that in Fig. 15 (I-a) to (I-c). In addition, the reflection wavelength of each FBG can be measured as a vibration change of the same phase, and it can be confirmed that this system can continue stable real-time measurement without data loss. Based on the above, we developed a multichannel FBG measurement system with measurement time resolution of 9.9 μs and realized real-time sensing by introducing delay-correction processing.

IV. Conclusion

We developed a measurement system using an FPGA, which realized high-speed multichannel measurement of multiplexed FBGs. The FDML laser was operated at a sweep frequency of 50.7 kHz, and enabled bidirectional high-speed wavelength sweeping with a sweep band of 60 nm. In the signal-processing system with an installed FPGA, FBG signals on multiplexed channels could be processed in parallel and in real-time, at a sampling frequency of 250 MHz. A digital circuit for detecting the centroid peak was designed and installed inside the FPGA, realizing high-speed and high-resolution detection of the FBG. The measurement system enabled simultaneous measurement of 15 FBGs with multiplexed channels, using the FDML laser. This study showed that the influence of the delay due to the optical fiber length reduced the accuracy of the measured wavelength. The proposed delay-correction process had the following advantages: a special optical system for correction was not required, the calculation cost for real-time processing was low, and it was applicable to multichannel systems. We showed that the measurement system introducing this correction process could measure multiplexed FBGs in real-time with a measurement time resolution of 9.9 μs, without being affected by the delay.

References

[1] J. M. Lopez-Higuera, Ed., *Handbook of Optical Fibre Sensing Technology*. Hoboken, NJ, USA: Wiley, 1997.

[2] A. D. Kersey *et al.*, "Fiber grating sensors," *J. Lightw. Technol.*, vol. 15, no. 8, pp. 1442–1463, Aug. 1997.

[3] A. Othonos and K. Kalli, *Fiber Bragg Grating*. Norwood, MA, USA: Artech House, 1999.
[4] J. M. Lopez-Higuera, L. R. Cobo, A. Q. Incera, and A. Cobo, "Fiber optic sensors in structural health monitoring," *J. Lightw. Technol.*, vol. 29, no. 4, pp. 587–608, Feb. 15, 2011.
[5] N. Takeda, Y. Okabe, J. Kuwahara, S. Kojima, and T. Ogisu, "Development of smart composite structures with small-diameter fiber Bragg grating sensors for damage detection: Quantitative evaluation of delamination length in CFRP laminates using Lamb wave sensing," *Compos. Sci. Technol.*, vol. 65, nos. 15–16, pp. 2575–2587, Dec. 2005.
[6] G. Wild and S. Hinckley, "Acousto-ultrasonic optical fiber sensors: Overview and state-of-the-art," *IEEE Sensors J.*, vol. 8, no. 7, pp. 1184–1193, Jul. 2008.
[7] H. Tsuda *et al.*, "Acoustic emission measurement using a strain-insensitive fiber Bragg grating sensor under varying load conditions," *Opt. Lett.*, vol. 34, no. 19, pp. 2942–2944, Oct. 2009.
[8] A. Wada, S. Tanaka, and N. Takahashi, "Optical fiber vibration sensor using FBG Fabry–Pérot interferometer with wavelength scanning and Fourier analysis," *IEEE Sensors J.*, vol. 12, no. 1, pp. 225–229, Jan. 2012.
[9] K.-S. Kim, Y. Mizuno, and K. Nakamura, "Fiber-optic ultrasonic hydrophone using short Fabry–Pérot cavity with multilayer reflectors deposited on small stub," *Ultrason.*, vol. 54, no. 4, pp. 1047–1051, Apr. 2014.
[10] S. H. Yun, D. J. Richardson, and B. Y. Kim, "Interrogation of fiber grating sensor arrays with a wavelength-swept fiber laser," *Opt. Lett.*, vol. 23, no. 11, pp. 843–845, Jun. 1998.
[11] T. Saitoh, K. Nakamura, Y. Takahashi, H. Iida, Y. Iki, and K. Miyagi, "Ultra-long-distance fiber Bragg grating sensor system," *IEEE Photon. Technol. Lett.*, vol. 19, no. 20, pp. 1616–1618, Oct. 15, 2007.
[12] Y. Shinoda, T. Arai, D. Miyata, and T. Higo, "Real-time measurement of static strain using fiber Bragg gratings with optical frequency domain reflectometry," in *Proc. SICE Annu. Conf.*, Sep. 2011, pp. 1870–1873.
[13] K. Yuksel, V. Moeyaert, P. Megret, and M. Wuilpart, "Complete analysis of multireflection and spectral-shadowing crosstalks in a quasi-distributed fiber sensor interrogated by OFDR," *IEEE Sensors J.*, vol. 12, no. 5, pp. 988–995, May 2012.
[14] R. Huber, M. Wojtkowski, K. Taira, J. G. Fujimoto, and K. Hsu, "Amplified, frequency swept lasers for frequency domain reflectometry and OCT imaging: Design and scaling principles," *Opt. Express*, vol. 13, no. 9, pp. 3513–3528, May 2005.
[15] R. Huber, M. Wojtkowski, and J. G. Fujimoto, "Fourier domain mode locking (FDML): A new laser operating regime and applications for optical coherence tomography," *Opt. Express*, vol. 14, no. 8, pp. 3225–3237, Apr. 2006.
[16] E. J. Jung *et al.*, "Characterization of FBG sensor interrogation based on a FDML wavelength swept laser," *Opt. Express*, vol. 16, no. 21, pp. 16552–16560, Oct. 2008.
[17] D. Chen, C. Shu, and S. He, "Multiple fiber Bragg grating interrogation based on a spectrum-limited Fourier domain mode-locking fiber laser," *Opt. Lett.*, vol. 33, no. 13, pp. 1395–1397, Jul. 2008.
[18] B. C. Lee, E. J. Jung, C. S. Kim, and M. Y. Jeon, "Measurement science and technology dynamic and static strain fiber Bragg grating sensor interrogation with a 1.3 μm Fourier domain mode-locked wavelength-swept laser," *Meas. Sci. Technol.*, vol. 21, no. 9, Sep. 2010, Art. no. 094008.
[19] T. Yamaguchi and Y. Shinoda, "Real-time fiber Bragg grating measurement system using temperature-controlled Fourier domain mode locking laser," *Opt. Eng.*, vol. 56, no. 6, Jun. 2017, Art. no. 066112.
[20] T. Yamaguchi and Y. Shinoda, "Multichannel high-speed fiber Bragg grating interrogation system utilizing a field programmable gate array," *IEEE Sensors Lett.*, vol. 2, no. 1, Mar. 2018, Art. no. 5500204.
[21] Q. Liu *et al.*, "High-speed interrogation system of multi-encoding weak FBGs based on FDML wavelength swept laser," *Opt. Laser Technol.*, vol. 107, pp. 54–58, Nov. 2018.
[22] E. Monmasson and M. N. Cirstea, "FPGA design methodology for industrial control systems—A review," *IEEE Trans. Ind. Electron.*, vol. 54, no. 4, pp. 1824–1842, Aug. 2007.
[23] P. M. Watts, R. Waegemans, Y. Benlachtar, V. Mikhailov, P. Bayvel, and R. I. Killey, "10.7 Gb/s transmission over 1200 km of standard single-mode fiber by electronic predistortion using FPGA-based real-time digital signal processing," *Opt. Express*, vol. 16, no. 16, pp. 12171–12180, Aug. 2008.
[24] Z. Li, M. Liu, Y. Wang, Q. Liu, and J. Gong, "Delay calibration method for wavelength-swept laser-based FBG demodulation system," *IEEE Photon. Technol. Lett.*, vol. 26, no. 20, pp. 2090–2092, Oct. 15, 2014.
[25] J. Mei, X. Xiao, and C. Yang, "Delay compensated FBG demodulation system based on Fourier domain mode-locked lasers," *IEEE Photon. Technol. Lett.*, vol. 27, no. 15, pp. 1585–1588, Aug. 1, 2015.

Tatsuya Yamaguchi (M'18) received the B.S., M.S., and Ph.D. degrees from Nihon University, Tokyo, Japan, in 2013, 2015, and 2018, respectively, all in engineering.

He joined the Department of Electrical Engineering, Nihon University. His current research interests include optical measurements, digital signal processing, structural health monitoring, and optical fiber sensing.

Dr. Yamaguchi is a member of the Institute of Electrical Engineers of Japan (IEEJ), the Society of Instrument and Control Engineers (SICE), and the International Society for Optical Engineering (SPIE).

Keisuke Ishihara (S'19) received the B.S. degree in engineering from Nihon University, Tokyo, Japan, in 2017, where he is currently pursuing the M.S. degree.

His current research interests include optical measurements, optical coherence tomography, and optical fiber sensing.

Mr. Ishihara is a Student Member of the Institute of Electrical Engineers of Japan (IEEJ).

Yukitaka Shinoda (M'15) received the B.Sc., M.Sc. and Ph.D. from Nihon University, in 1987, 1989 and 2004, respectively, all in electrical engineering.

He was a Visiting Researcher of the Virginia Polytechnic Institute and State University (Virginia Tech), from 2009 to 2010. Since 2013, he has been a Professor with the College of Science and Technology, Nihon University. He has focused on laser sensing, digital signal processing, motion analysis, and optical scanning holography.

Dr. Shinoda is a member of the Institute of Electrical Engineers of Japan (IEEJ), the Society of Instrument and Control Engineers (SICE), the Japan Society of Applied Physics (JSAP), and the International Society for Optical Engineering (SPIE).